United States Department of Commerce
Technology Administration
National Institute of Standards and Technology

NIST Technical Note 1381

Rapid Evaluation of Mode-Stirred Chambers Using Impulsive Waveforms

John M. Ladbury
Robert T. Johnk
Arthur R. Ondrejka

NIST Technical Note 1381

Rapid Evaluation of Mode-Stirred Chambers Using Impulsive Waveforms

John M. Ladbury
Robert T. Johnk
Arthur R. Ondrejka

Electromagnetic Fields Division
Electronics and Electrical Engineering Laboratory
National Institute of Standards and Technology
325 Broadway
Boulder, Colorado 80303-3328

June 1996

U.S. DEPARTMENT OF COMMERCE, Michael Kantor, Secretary
TECHNOLOGY ADMINISTRATION, Mary L. Good, Under Secretary for Technology
NATIONAL INSTITUTE OF STANDARDS AND TECHNOLOGY, Arati Prabhakar, Director

National Institute of Standards and Technology Technical Note
Natl. Inst. Stand. Technol., Tech. Note 1381, 40 pages (June 1996)
CODEN:NTNOEF

U.S. GOVERNMENT PRINTING OFFICE
WASHINGTON: 1996

For sale by the Superintendent of Documents, U.S. Government Printing Office, Washington, DC 20402-9325

RAPID EVALUATION OF MODE-STIRRED CHAMBERS USING IMPULSIVE WAVEFORMS

John M. Ladbury, Robert T. Johnk, and Arthur R. Ondrejka

Electromagnetic Fields Division
Electronics and Electrical Engineering Laboratory
National Institute of Standards and Technology
Boulder, Colorado 80303

In this paper, we present an experimental technique for the rapid evaluation of mode-stirred (or reverberation) chambers. The measurement provides an estimate of the average chamber quality factor (Q) by measuring the chamber impulse response and observing the decay of the spectral components of the response. The results show good agreement with those obtained using conventional CW techniques. The measurement is well suited for low-frequency analysis of a chamber, where costly and time consuming mode-tuned approaches are generally employed. Since this technique does not use paddle stirring, the time required to evaluate a chamber can be significantly reduced.

Key words: Decay time; impulse response; integrated impulse response; mode-stirred chambers; Q; quality factor; reverberation chambers; short time Fourier transform; time-domain; time-frequency analysis; windowed Fourier transform

1. Introduction

We propose a method for estimating the quality factor (Q) of a mode-stirred chamber by exciting the chamber with an impulse and measuring the decay time of the electric field in the chamber for frequencies in a narrow band. This is accomplished by passing the resulting impulse response through a short-time Fourier transform (STFT), and observing the decay rate of the various spectral components. First, however, we will give a brief description of mode-stirred (or reverberation) chambers in general, as well as the traditional methods which have been employed for their evaluation.

Electromagnetic reverberation chambers provide an excellent environment for immunity testing [1-3] and have recently been employed for emissions testing as well [3,4]. Before any chamber can be used, it must be carefully evaluated so that the field intensity inside the chamber as a function of input power can be estimated. It is therefore necessary to obtain an estimate of the chamber quality factor Q. The quality factor is important because it measures the ability of a chamber to store modal energy in the form of high field strengths. Q is defined as

$$Q = \omega_0 \frac{\textit{Stored energy}}{\textit{Dissipated power}}, \tag{1}$$

where ω_0 is the excitation (angular) frequency [1,2].

The traditional method for measuring chamber Q is shown in figure 1. The net input power P_t and the received power P_r are measured, and a calculated value Q' is given as [1]

$$Q' \approx 16\pi^2 \frac{V}{\lambda^3} \frac{P_r}{P_t}, \tag{2}$$

where V is the chamber volume in cubic meters, and λ is the wavelength in meters. Since Q depends on the specific cavity mode excited in the chamber, the modes must be "mixed" or "stirred" to excite other modes. This may be done either by changing the chamber boundary conditions [1-5] or by changing the drive frequency [6,7]. Whatever technique is used, the results must be weighted and combined in some fashion to generate a representative value. This method is useful when the chamber has a simple geometric shape and V is easy to calculate. Complex shapes, however, make this approach impractical.

Another method, which does not require an estimate of the chamber volume, is used in acoustical reverberation chambers [8-11] but has not been widely used in electromagnetic reverberation chambers. This method involves observation of the transient response of the chamber and evaluation of parameters based on those observations. For example, the decay rate of the transient response is directly related to the quality factor of the chamber, as shown below.

Jackson [12] shows that if a single mode in a cavity is excited, once the exciting function is turned off, the electric field $E(t)$ will decay exponentially as

$$E(t) = E_0 e^{-\frac{\omega_0 t}{2Q}} e^{-j(\omega_0 + \Delta\omega)t} = E_0 e^{-\frac{t}{2\tau}} e^{-j(\omega_0 + \Delta\omega)t}, \tag{3}$$

where E_0 is the initial electric field magnitude, τ is the exponential decay time, and $(\omega_0 + \Delta\omega)$ represents the fact that the oscillation is not a pure frequency, but a superposition of frequencies about ω_0. Thus, we could measure $E(t)$ and calculate the decay time τ from the measured data. From τ and eq (3), we can calculate Q as

$$Q = \omega_0 \tau. \tag{4}$$

Unfortunately, it may not be possible to excite just a single mode in a complex environment such as a reverberation chamber, especially at higher frequencies. This is because the spacing between modes decreases as frequency increases [1]. If multiple modes are excited, the electric field can be represented by the superposition of several exponentially decaying sinusoidal functions of the same form as eq (3):

$$E(t) = \sum_{k=0}^{M-1} E_k e^{-\frac{\omega_k t}{2Q_k}} e^{-j(\omega_k + (\Delta\omega)_k)t} = \sum_{k=0}^{M-1} E_k e^{-\frac{t}{2\tau_k}} e^{-j(\omega_k + (\Delta\omega)_k)t}, \tag{5}$$

where M is the number of modes excited, the subscript k refers to the kth mode excited in the cavity, and the notation $(\Delta\omega)_k$ indicates that each mode can have a unique bandwidth. Liu et al. [13] show theoretically that, for a narrow band of frequencies, if δ_s is the skin depth of the chamber walls, the values of $1/(Q_k \delta_s)$ are tightly grouped about a central value. From this, we can deduce that the values of the decay rates $1/\tau_k$ will also be tightly grouped. If they are assumed to be constant, the electric field can be approximated as

$$E(t) \approx e^{-\frac{t}{2\tau}} \sum_{k=0}^{M-1} E_0 e^{-j(\omega_k + (\Delta\omega)_k)t}. \tag{6}$$

Thus, the electric field is a decaying exponential times an unknown modulating function, which is caused by the beating of the various modes against each other, as well as other interference effects. This modulation is well known in the acoustical literature [10,11], where similar results have been obtained in acoustical reverberation chambers and the measured parameter is sound pressure rather than electric field.

Another approach showing the exponential decay of a transient signal is given in [14]. Here, the authors assume a uniform energy distribution throughout the chamber and also assume that the loss of energy due to imperfect conductors in the chamber walls is proportional to the instantaneous value of the total energy in the cavity. The resulting differential equation also results in an exponential decay of the chamber energy.

Our method is described in the remainder of this paper. Section 2 gives a detailed description of the equipment setup, Section 3 describes the data processing involved, and Section 4 shows our experimental results. In Section 5 we review the advantages and limitations of our proposed method, discuss new questions which have been raised by our results, and recommend improvements and future endeavors which should improve our understanding of mode-stirred chambers.

2. Equipment Setup

The system's transient response was measured using the setup shown in figure 2. The test chamber was the NIST mode-stirred chamber, with the paddle removed. This chamber is made of steel and has dimensions of 3.05 m by 4.57 m by 2.74 m. An impulse generator with a bandwidth of approximately 1 GHz drives a transverse electromagnetic (TEM) horn antenna, which is placed inside the National Institute of Standards and Technology (NIST) reverberation chamber. A second TEM horn inside the chamber measures the continuous time impulse response $x(t)$, and a high-speed digitizing oscilloscope records the results. A measurement delay t_0 of 150 ns was present in the oscilloscope, and will show up in all plots of data versus time. The oscilloscope sampled the response with a period T of 40 ps per point, which gave an effective measurement bandwidth of 12.5 GHz, so aliasing was not a problem. The duration of the impulse response was between 4.5 μs and 6 μs. Technically, the duration of the impulse response is infinite, but for practical reasons we are interested only in the portion of the response where the signal is greater than the noise floor. In an effort to be conservative, data were captured over a full 6 μs range, but only the first 4.5 μs of data were used for the subsequent processing and parameter estimation. To capture the entire record, 150 000 data points were measured by the oscilloscope. This was accomplished by measuring 60 records, each 5000 points or 200 ns long, and shifting the origin of each record by 100 ns. The number of averages per record and the oscilloscope sensitivity were kept constant for each record in an effort to avoid changes in measurement characteristics from record to record. We then combined the records by averaging the overlapping time segments in each record to produce a final record of length 152 500 points. The first 2500 points and the last 2500 points of this final record are not averaged, since there was no overlap. The final record is shown in figure 3. If we assume that the receiving antenna's response is roughly proportional to the electric field amplitude in the vicinity of the antenna, then the decay rate of the voltage in any given frequency band should be identical to the decay rate of the field inside the chamber. For this reason, all subsequent processing will be performed on the output voltage waveform, and the results will be assumed to be applicable to the fields inside the chamber.

The number of captured records could be reduced by a factor of 2 if no overlap is allowed. In this measurement, the overlapped regions were used to verify the oscilloscope timing and noise amplitude by comparing the data in each region. Poor agreement would show that the signal has decayed below the noise floor of the measurement system or that the time stability of the system was not sufficient for this measurement. Analysis of the data showed that this was not a problem for our system. There was an expected decrease in sensitivity in the later records due to the decaying nature of the signal, but agreement remained excellent throughout the entire measurement time. Based on these observations, we think that future measurements can be made without the redundancy in the data. Even without the redundancy, the amount of data required for the measurement remains formidable.

3. Data Processing

The sampled data were processed using a sliding-window fast Fourier transform (FFT), also known as a short time Fourier transform or spectrogram [15-17]. The FFT is simply a method of calculating the discrete Fourier transform (DFT) at several frequencies simultaneously, and the sliding window provides an estimate of the spectral content of a signal as a function of time, similar to passing the signal through a bank of band-pass filters. The equation for the windowed DFT of a discrete signal x is given by

$$X_n = \sum_{i=0}^{N-1} x_i\, w_i\, e^{\frac{-j2\pi n i}{N}}. \tag{7}$$

In this equation, N is the window width, or number of points from the original signal used in calculating X_n, n selects the central frequency $f = n/NT$, with T defined previously, and w_i is the window weight, described below. The frequency resolution and bandwidth of the transform are determined by the value of N. For the DFT, the frequency resolution R is equal to the bandwidth BW and is given by

$$BW = R = \frac{1}{NT}. \tag{8}$$

In order to generate values of X_n as a function of time, we must introduce an offset into the equation:

$$X_{n,k} = \sum_{i=0}^{N-1} x_{k+i}\, w_i\, e^{\frac{-j2\pi n i}{N}}. \tag{9}$$

Here, k selects the time associated with a particular transform, $t = kT + t_0$.

The squared magnitude $|X_{n,k}|^2$ of the output gives an estimate of the spectral power contained in the signal. For our purposes, the parameters we are interested in are based on the shape of the waveform, not the amplitude. For this reason, the plots for all decay records given in this report are measured in relative power, and no axis labels are given. This convention allows us to plot multiple decay records in a single figure and separate them vertically.

The time response of the output signal is greatly influenced by the window shape w_i and the window size, N. The window shape associated with spectrographic analysis has been thoroughly analyzed and documented [16-18]. The consensus is that windows should gradually taper to zero or nearly zero at the endpoints. This results in smooth data, but compromises the ability to respond to abrupt changes in the signal. The window we chose, the Hanning window, was selected on the basis of simplicity and ease of implementation, and is given below:

$$w_i = \frac{1}{2} - \frac{1}{2}\cos\left(\frac{2\pi i}{N-1}\right) \qquad for \quad i = 0,\ 1,\ ...,\ N-1. \tag{10}$$

Figure 4 shows the effect of using a tapered window and a simple rectangular window ($w_i = 1$) for a frequency of 500 MHz and $N = 5000$. The relative smoothness of the data processed with a Hanning window demonstrates the improvements gained by windowing. The long-term characteristics of the two signals are very similar, however. Thus, it appears that window shape will not significantly influence the measurement of the decay time. Many of the figures shown in this paper are calculated for a central frequency of 500 MHz. These figures are representative of our data in general, except where noted.

The window size plays a greater role in the processing of the decay records. Large values of N accentuate long-term phenomena and give better frequency resolution than small values, which are better at tracking rapid changes in signal characteristics. Ideally, since we are interested in modal decays, a large value of N should be used to examine the long-term narrow-band characteristics, as mentioned by Carin and Felsen [15]. Unfortunately, it is possible to make N too large. Figure 5 shows two plots of $|X_{n,k}|^2$ versus time for a central frequency of 500 MHz and windowed using a Hanning window. The smooth plot was generated with $N = 10\ 000$, and the coarse plot was generated from the same source data, but with $N = 500$. While the curve with $N = 10\ 000$ is smoother, the exponential decay characteristic of the other curve is more apparent. This can be explained by the fact that a longer window slows the maximum rate of modulation of the signal and increases the correlation between nearby points, and as a result, there is less information about the signal characteristics as a function of time. In contrast, a narrow window allows rapid modulation and shorter correlation times, which improves our ability to extract the decay time from the data. For this reason, we chose the narrowest window possible while maintaining our minimum desired frequency resolution for most of our processing, except where noted. Since we wished to generate data every 50 MHz, a spacing of $N = 500$ was selected.

The correlation caused by the sliding window can be used to our advantage. Since adjacent points of $X_{n,k}$ cannot change abruptly, it is not necessary to calculate values of $X_{n,k}$ for all values of k. We determined experimentally that, given a window width N, we can increase the sample time of $X_{n,k}$ from T to $NT/10$ without compromising apparent signal resolution.

Once a window size and shape have been selected, the data must be processed to produce an estimate of the decay time. Although there is an apparent linear (exponential) trend to the data, it is difficult to select a line of best fit. (From this point on, when we refer to a linear trend, we will be referring to the linear decay of the data when plotted on a semi-logarithmic graph, as shown.) A least-squares regression analysis on this raw data is possible, but several problems present themselves. First, deep nulls at either end of the series can drastically affect the final parameter estimates. Second, if the data depart from the ideal decay model, it will be difficult to detect. Finally, linear regression may produce good results for a wide variety of applications, but data must have a roughly gaussian spread about the central line if we wish to generate a maximum likelihood estimate of the decay parameters [18]. This obviously is not the case for the data presented here. For these reasons, the data should be smoothed before any regression analysis is performed. Several types of smoothing, such as time averaging, frequency averaging, and spatial averaging are possible. In addition to these methods, an integrated impulse response method (IIRM) [19,20] can be applied after or instead of the other methods. These methods, as well as the advantages and disadvantages of each, are described below. Any of these methods can be combined to produce additional smoothing.

3.1 Time Averaging

Time averaging involves passing a time sequence through a low-pass filter. The most simple and often used example is the moving average filter, where a data point is replaced with the average of itself and a fixed number of its neighbors:

$$\tilde{X}_{n,k} = \frac{1}{2L+1} \sum_{j=k-L}^{k+L} X_{n,j}, \tag{11}$$

where $\tilde{X}$ is the resultant time averaged data and L is the number of neighbors on each side of the data point included in the average. Since the sample periods for $X_{n,k}$ may vary for different window widths, it is more convenient to refer to an averaging time Δ. If we represent the sample period of $X_{n,k}$ as T_X, then the averaging time is $\Delta = 2LT_X$.

Figure 6 shows a plot of time-averaged spectral power versus time for a central frequency of 500 MHz. Also plotted is the moving average of the data for various values of Δ, along with the line which best fits the moving average data. An exponential curve fit to the original data results in a similar decay rate. Therefore, the moving average makes the data appear more attractive, but does not significantly change the results. The primary advantage to this method is the ease of implementation. The disadvantage is that the amount of smoothing is directly related to the value of Δ. Large values of Δ result in smooth data, but tend to disguise important characteristics of the signal, such as changes in decay time.

The noise floor of the measurement system is revealed by a flattening of the decay curve. No obvious flattening was observed for frequencies below 1 GHz, and we therefore assume that the dynamic range of the system was adequate for this frequency range. Above 1 GHz, however, the system becomes less efficient for both transmission and reception, and the noise floor becomes apparent. Figure 7 shows the limitations of the measurement due to noise for a decay record with a central frequency of 3 GHz. The flattened response in the last half of the decay record is characteristic of the records we processed above 2 GHz. The relative noise amplitude could be improved by using a pulse generator and antennas designed for higher frequency applications.

3.2 Frequency Averaging

Frequency averaging is closely related to time averaging. Instead of averaging adjacent time samples, adjacent frequency samples are averaged:

$$\bar{X}_{n,k} = \frac{1}{2D+1} \sum_{i=n-D}^{n+D} X_{i,k}, \tag{12}$$

where $\bar{X}$ is the frequency averaged data. From eq (8), a single point has a bandwidth equal to the frequency resolution R of the DFT, so the approximate averaging bandwidth of $\bar{X}$ is $R(2D + 1)$.

Figure 8 shows frequency averaged data for a central frequency of 500 MHz, $N = 500$, and averaging bandwidths of 50 MHz (no averaging), 150 MHz, 250 MHz, and 550 MHz.

The frequency averaging method is based on the assumption that each of the decay records $X_{n,k}$ have similar characteristics, that is, similar values for initial power, decay time, and decay characteristics. It may be possible to correct for variations due to measurement system effects by compensating for the nonideal characteristics of the transmitted signal, but these will only compensate for variations in incident power; reflected power from a time-domain signal is difficult to measure and correct. The assumptions of similarity between records are realistic as long as the frequencies are close, but close is defined somewhat arbitrarily. For these reasons, frequency averaging must be used with great caution. These same assumptions must also be valid for any other technique as well. Since the DFT has a nonzero bandwidth, the signal characteristics must be assumed constant across the passband. The frequency band in question is generally narrower than that associated with frequency averaging, so the assumptions are easier to justify.

Despite these drawbacks, frequency averaging has strong advantages. Hill [6] shows that frequency averaging improves the spatial uniformity of the field, and also reduces the interaction between the transmitting antenna and the chamber walls in a two dimensional chamber. (This is yet to be experimentally verified in a three-dimensional chamber.) Also, it is not necessary to acquire as much data for frequency averaging as for the other techniques, as described below.

It is possible to overcome some of the problems associated with long time windows: long windows result in greater frequency resolution and therefore allow more decay records to be averaged over a given bandwidth. An example of the effects of frequency averaging on data processed with a long window ($N = 5000$) is shown in figure 9 with averaging bandwidths which are substantially smaller than those used in figure 8. These figures show that frequency averaging works best for data processed with long windows. This is caused by the improved frequency resolution associated with long windows. For example, as shown before, a 500-point window has an effective bandwidth of 50 MHz, so averaging over a 50 MHz bandwidth results in only a single point, and no averaging. A 5000-point window has an effective bandwidth of 5 MHz, so averaging over a 50 MHz bandwidth allows 10 points to be averaged together. Thus, if we restrict ourselves to a specific bandwidth and either time averaging or frequency averaging, then frequency averaging with long windows appears to give better results.

Figure 9 shows another advantage of frequency averaging. If the fluctuations about the central trend line are small enough, then it is not necessary to acquire as much data. If we were to estimate the decay time from only two samples on this curve, shown as X on figure 9, the estimate of τ is 538 ns rather than 547 ns, or a difference of less than 2 percent. Thus it is possible to estimate the decay time by capturing only 2 records, instead of the 60 records required for the other methods mentioned here. This is an extreme example and very sensitive to small errors in the measurement of the two points. The fact that these two methods agree so well should not be viewed as an indication of how well similar results would agree, but it demonstrates the potential strength of the technique. Obviously, we lose the fine detail and any opportunity to observe multiple decay characteristics. We therefore recommend additional measurements to verify the results, but for well-behaved environments, this is a practical alternative. This technique was introduced by Johnk and Ondrejka [21] for use in aircraft and anechoic chambers, and is the precursor to the work presented in this paper.

3.3 Spatial Averaging

Spatial averaging requires multiple records, one for each of several antenna configurations, to be captured and processed as described above. Alternatively, records can be captured for each of several different paddle positions, which yields similar results. Once the records have been processed, the various $X_{n,k}$ must be averaged together, resulting in a smoother curve. Since this method can make use of narrow bandwidths, it is not as sensitive to some of the assumptions associated with the other techniques, and it is therefore possible to avoid some of the pitfalls associated with frequency averaging. The chamber characteristics should be the same for each measurement, so the risks of one measurement masking the characteristics of another should not be present. The smoothing effects should be comparable to those presented for frequency averaging, but it is possible to obtain these results over a narrow frequency range.

The primary disadvantage of spatial averaging is the increase in complexity and data. The antennas must be moved by the person making the measurement or by a mechanical positioning system. Spatial averaging significantly increases the storage requirements of the processing computer, as well as processing time, because the data must be processed for each configuration. This limitation may be reduced somewhat by taking fewer records and relying on the smoothing effect of spatial averaging, as in frequency averaging. It would still require a substantial effort to collect and process the data. For these reasons, this method was not tested and is mentioned here only for completeness. We hope to present results in a future paper.

Spatial averaging is roughly equivalent to frequency averaging. Pierce [8] analyses the statistics associated with both spatial and frequency averaging, and gives estimates of the possible reductions in measurement variance associated with each method. These estimates could be used to show the relationship between averaging bandwidth and number of independent measurements, and how to combine these techniques, if desired. Johnk and Ondrejka [21] have shown that frequency averaging and paddle stirring give similar improvements to the measured data, and the combination of both methods yields additional improvements.

3.4 Integrated Impulse Response Method

Another method of time smoothing, known as the Integrated Impulse Response Method, was presented by Schroeder [19]. Schroeder suggests integrating a modulated decaying exponential signal $u(t)$ as follows:

$$P[u(t)] = \int_{t}^{\infty} u(\tau)d\tau. \tag{13}$$

Given the sampled nature of our data, we can approximate the integral as a sum:

$$(P[\boldsymbol{u}])_k = \sum_{l=k}^{\infty} u_l, \tag{14}$$

where $\boldsymbol{u}$ is the sampled version of $u(t)$, u_i is the ith sample of $\boldsymbol{u}$, and $(P[\boldsymbol{u}])_k$ is the kth sample of $P[\boldsymbol{u}]$. If $\boldsymbol{u}$ is the squared magnitude of the DFT of our chamber response, then all values of $\boldsymbol{u}$ will be nonzero, and ***P*[*u*]** will be monotonically decreasing. This feature alone should improve the smoothness of the curve.

Another approximation must be made because we do not know values of $u(t)$ for all future times. If we truncate the integral (sum) at some finite value t_1 (K), we have

$$(P[u])_k = \sum_{t=k}^{K-1} u_t \ . \tag{15}$$

This will introduce an error because the value of the sum must approach zero as k approaches K. We can analyze the effect of this error on the estimation of the decay time by assuming the $u(t)$ is an ideal decaying exponential $e^{-t/\tau}$. Truncation of the integral results in a multiplicative error α given by

$$\alpha = 1 - e^{(t-t_1)/\tau}. \tag{16}$$

This error term is strictly decreasing for $t < t_1$, and any decay time based on the truncated integral will be biased below the actual value of τ. The bias will be greatest near $t = t_1$, and for large values of τ. We can minimize the bias by analyzing only the data for $t \ll t_1$. Unfortunately, this has the disadvantage of reducing the amount of data available for estimating τ. As a compromise, we would like to find a processing range for t that allows enough data for estimating τ but is sufficiently separated from t_1. We can solve eq (16) for $(t-t_1)$:

$$(t-t_1) = \tau \ln(1-\alpha). \tag{17}$$

Equation (17) gives an estimate of the time constraints we must place on the least-squares regression estimate of τ; that is, we must only evaluate the data for $t < t_1 + \tau \ln(1-\alpha)$. This requires an initial estimate of τ, which can be calculated using one of the other techniques, estimated from early data, or evaluated iteratively. We must also select an allowable value for α. The parameters we used were determined by trial and error. For our measurements, we used a value of $t_1 = 4.5$ μs and estimated τ based on the data for $t < 3.5$ μs. The longest observed decay time was 748 ns, which corresponds to $\alpha \approx 0.74$. For an ideal exponential, these parameters resulted in a bias of less than 5 percent, which was considered acceptable.

Once an estimate of τ has been obtained, it is possible to estimate the bias introduced by the truncation and correct for it, if necessary, by adding our estimate of $\boldsymbol{P}[\boldsymbol{u}]_K$ to $\boldsymbol{P}[\boldsymbol{u}]$. This results in forcing the endpoint of $P[u]$ to match the endpoint of our exponential curve fit. This may seem like cheating, but the result is more accurate than assuming that $P[u]$ is actually equal to 0 for $k \geq K$.

Figure 10 shows the effect of using the integrated impulse response method on the raw data calculated at 500 MHz. No additional smoothing is required other than the IIRM. The IIRM appears to work best on data processed with a short window. Figure 11 shows data for a central frequency of 500 MHZ, $N = 10\,000$, processed with the IIRM. The fluctuations about the central line are greater, but the results are still useful.

4. Experimental Results

Decay time was calculated for several frequencies using the IIRM with $N = 500$, $t_1 = 4.5$ μs, and $t < 3.5$ μs. A graph of decay time versus frequency is given in figure 12. These results were used to calculate Q based on eq (4) given in Section 1. We compared our results with those calculated using traditional measurement techniques [1], and both sets of data are presented in figure 13. The traditional technique provides estimates for the maximum, minimum, and average values of Q. The maximum estimate corresponds to the maximal coupling between the transmit and receive antennas over several paddle positions. The minimum corresponds to the minimal coupling, which could be zero or nearly zero in some configurations, and are therefore not presented. These conditions usually occur only at specific paddle positions and therefore do not represent the general chamber characteristics. We therefore assumed that our data would correspond best with the average estimate of Q, and the graph seems to validate this assumption.

Our estimates of Q are substantially higher in the low frequency range, below about 300 MHz. We hope to address this difference in the future. The modal density is low below 300 MHz, and it is possible that the antennas cannot couple to all of the modes which are present, and the results using the traditional techniques would probably be biased on the low side. Also, the error bounds associated with measurements in the NIST mode-stirred chamber are greater than 8 dB below 300 MHz, and according to personal communications with G.H. Koepke at

NIST in Boulder, recent measurements demonstrate a change in chamber statistics below 300 MHz due to the limited number of modes below this frequency. Another possibility is that some unknown property of the chamber is influencing the results. Figure 14 shows the decay record at 200 MHz. Two distinct decay rates are apparent, with substantially different decay times and associated quality factors. A similar but smaller effect occurs at 250 MHz. One possible explanation of this result is based on the work of Hill et al. [14] which shows that two primary loss mechanisms will determine the quality factor of an empty chamber: antenna losses (power dissipated by antenna loads) and wall losses (power dissipated by resistive losses in the walls). Antenna losses dominate at lower frequencies and wall losses dominate at higher frequencies. Once a large number of modes have been set up inside a chamber, those modes that couple strongly to the antennas will decay at a different rate than those modes that are weakly coupled to the antennas. Thus, at frequencies where antenna losses dominate, there should be an initial rapid decay as the power in the strongly coupled modes is dissipated, followed by a slower decay caused by a combination of week coupling to the antennas and wall losses. The decay time values in figure 12 and the Q values in figure 13 were calculated with a linear regression based on the first 3.5 μs of the decay record. If there are two distinct decay rates, evaluating the entire record will result in an estimate of τ between the estimates based on the rapid decay or slow decay portions only. The entire record resulted in an estimates of $\tau = 537$ ns and $Q = 675$. If we base our estimates on the slow decay portions only, we obtain estimates of $\tau = 586$ ns and $Q = 736$. If the faster decay is used, then our estimates will be $\tau = 373$ ns and $Q = 469$. Based on these observations, estimates based on the initial rapid decay result in Q values that are closer to those measured using traditional techniques. Unfortunately, this means that there is less information available for making our estimate. If this analysis is correct, heavy loading by the antennas may result in such a rapid decay that we cannot make accurate estimates of chamber Q, and that this technique is valid only for those frequencies where wall losses dominate the total loss inside the chamber.

In the mid-band range from 400 MHz to 800 MHz, our estimates are somewhat low. This could be due to the difference in antennas used in each type of measurement. The traditional technique used log-periodic antennas. Ours were resistively loaded TEM horns, which are larger and could easily load the chamber and lower the chamber Q. Even with these differences, the agreement is good, especially considering the tremendous differences in measurement techniques.

An estimate of the errors related to our measurement is based on the work of Davy [20]. In his paper, Davy gives an expression for the spatial variance of the decay rate $(1/\tau)$. This equation gives an estimate of the differences in decay rate which could be expected for various source and receive positions throughout an acoustical chamber, but the results are also applicable for electromagnetic measurements. These differences appear to be the dominant contributor to the uncertainty of our measurement. We will therefore concentrate on the spatial variance in this paper. The variance estimate is

$$\sigma_s^2 = var_s(\frac{1}{\tau}) = (\frac{10}{\ln 10})^2 \frac{12}{BW} (\frac{1}{\Lambda})^3 F(\frac{\ln 10}{10} D), \tag{18}$$

where BW is the bandwidth, Λ is the total time interval over which the exponential curve fit is calculated, D is the factor by which the power decays in Λ seconds, expressed in dB, and F is given by

$$F(x) = 1 - \frac{3}{x}(1+e^{-x}) - \frac{12}{x^2}e^{-x} + \frac{12}{x^3}(1-e^{-x}) . \tag{19}$$

If we assume that the values of $(1/\tau)$ are accurate within $\pm\sigma_s$, then, as a gross approximation, we can assume that the values of τ are accurate within $\pm 1/\sigma_s$, and Q is accurate within $\pm\omega_0/\sigma_s$. As an example, for the data at 500 MHz, processed with a window of 500 points, the bandwidth BW is 50 MHz, the observation time is approximately 3.5 μs, and over this time, the power decays by approximately $D = 30$ dB. Entering these values into the equation yields a value of σ_s^2 of $1.03 \cdot 10^{11}$. Given an estimate for $1/\tau$ of $1.82 \cdot 10^6$, this implies an accuracy of 18 percent; we estimate the uncertainty of our estimate of τ, and therefore Q, as also 18 percent. The estimated uncertainty of our data is shown in figure 15.

5. Conclusion and Recommendations

We have presented a method of evaluating the quality factor Q of an electromagnetic reverberation chamber. This method does not require tuner averaging, and gives results that appear quite similar to those obtained using traditional techniques. Several methods of processing the data were also presented, and each gave consistent results. Data processed with short time windows should be processed with one of two methods: time smoothing or the integrated impulse response method. Of these, the IIRM results in the greatest smoothing, but time smoothing is better suited for short time records where it is not possible to eliminate a portion of the data from the estimation process, as required with the IIRM. Frequency and spatial averaging were also addressed, and references were given which show that these two methods are roughly equivalent. Frequency averaging decreases the number of measurements required for accurate evaluations and uses a given bandwidth more effectively than time smoothing or the IIRM.

The combination of frequency averaging and the IIRM could perhaps be combined to provide better estimates of the decay time. The smoothing of frequency-averaged results could be further enhanced by the IIRM without loss of frequency resolution. We are examining the optimal values for the combination of window width N and averaging bandwidth, and will present results in a future report.

The test method can be extended to higher frequencies by using components which operate in the frequency band of interest, that is, high frequency antennas and a higher bandwidth impulse generator. The drawbacks of performing a high-frequency analysis of chambers using this test method are increased data requirements and lower sensitivity. The fact that higher frequencies are being generated and analyzed requires higher oscilloscope sample rates, which translates to more data. Increasing the bandwidth to 10 GHz results in a tenfold increase in the amount of data. Lower sensitivity results from the limited availability of high-speed high-amplitude impulse generators. Broad bandwidth generally implies low spectral energy content within any given passband, and measurements beyond approximately 10 GHz are not currently feasible given our existing measurement capabilities. Given the promising nature of transient measurement techniques, other related time-domain methods are being developed to overcome these difficulties.

Several recommendations which would improve the reliability of the measurements can be made. To improve the accuracy of our estimate of Q, it is important to reduce σ_s. Careful examination of eq (18) demonstrates the effect of changing any of the major parameters. The values of $F(\frac{\ln 10}{10}D)$ change very slowly for decays of D greater than 20 dB, thus the variance is dominated by the cubic term, and the best way to reduce the variance is to increase the measurement time. Unfortunately, the exponential decay of the signal means that sensitivity of the system decreases as we observe events farther away from the original impulse. If the oscilloscope is well calibrated, it may be possible to increase the sensitivity or averaging factor for later records and still be able to accurately recombine the records, but a thorough system analysis would be needed before the results could be considered reliable.

Through the course of this investigation, other questions which we hope to answer in the near future were raised. The effect of antenna type used in the measurements needs to be evaluated to see if commercially available antennas can be used instead of custom-made TEM horn antennas. This would make the technique more practical for industrial use and allow measurement of smaller facilities which are unable to hold a 1.2 m antenna.

The effect of absorbing material placed inside the chamber must also be evaluated. It is possible that this could result in nonlinear decay characteristics, as seen in acoustical measurements [22], or decay times that are too short to measure accurately. If the technique is applicable in loaded cavities, it may be possible to apply it to measurements such as aircraft immunity [21] and other high-cost applications.

This measurement technique has shown substantial advantages over the traditional methods for low-frequency analysis of reverberation chambers. The fact that these measurements can be performed without a mechanical stirrer or paddle means that a cavity can be evaluated before a mechanical stirrer is installed. By comparing the results before and after the installation of a mechanical stirrer, we can measure any degradation caused by the installation. Similarly, we can evaluate the effect of any change to the chamber, such as placing a test device or additional antennas into the chamber, *as it is made*. The effect of using a metallized paint or adding a zinc coating to walls can be easily measured before the work is completed, possibly saving time, effort, and money.

6. References

[1] Crawford, M.L.; Koepke, G.H. Design, evaluation, and use of a reverberation chamber for performing electromagnetic susceptibility/vulnerability measurements. Nat. Bur. Stand. (U.S.) Tech. Note 1092; 1986 April. 139 p.

[2] Hatfield, M.O.; Bean, J.L.; Freyer, G.J.; Johnson, D.M. Repeatability of mode-stirred chamber measurements. Proc. IEEE Intl. Symp. on EMC: 485-490; 1994.

[3] Hill, D.A.; Camell, D.G.; Cavcey, K.H.; Koepke, G.H. Radiated emissions and immunity of microstrip transmission lines: theory and measurements. Natl. Inst. Stand. Technol. Tech. Note 1377; 1995 June. 32 p.

[4] Page, J. Stirred mode reverberation chambers for EMC emission measurements and radio type approvals or organised chaos. IEE Intl. Conf. on Electromagnetic Compatibility: 313-320; 1994.

[5] Corona, P.; Latmiral, G.; Paolini, E. Performance and analysis of a reverberating enclosure with variable geometry. IEEE Trans. Electromag. Compat., EMC-22: 2-5; 1980.

[6] Hill, D.A. Electronic mode stirring for reverberation chambers. IEEE Trans. Electromag. Compat., EMC-36: 294-299; 1994.

[7] Loughry, T.A. Frequency stirring: an alternative approach to mechanical mode-stirring for the conduct of electromagnetic susceptibility testing. Phillips Laboratory, PL-TR--91-1036; 1991.

[8] Pierce, A.D. Acoustics - An Introduction to its Physical Principles and Applications. New York: McGraw-Hill; 1981.

[9] Vorlander, M., Bietz, H. Comparison of methods for measuring reverberation time. Acustica, 80: 205-215, 1994.

[10] Watson, R.B. The modulation of sound decay curves. J. Acous. Soc. Am. 18: 119-129; 1946.

[11] Morse, P.M.; Bolt, R. H. Sound waves in rooms. Rev. Mod. Phys. 16: 69-150; 1944.

[12] Jackson, J.D. Classical Electrodynamics. New York: John Wiley & Sons, Inc.; 1975.

[13] Liu, B.H.; Chang, D.C.; Ma, M.T. Eigenmodes and the composite quality factor of a reverberating chamber. Nat. Bur. Stand. (U.S.) Tech. Note 1066; 1983 August. 46 p.

[14] Hill, D.A.; Ma, M.T.; Ondrejka, A.R.; Riddle, B.F.; Crawford, M.T.; Johnk, R.T. Aperture excitation of electrically large, lossy cavities. IEEE Trans. Electromag. Compat. 36: 169-178; 1994.

[15] Carin, L.; Felsen, L.B. Wave-oriented data processing for frequency- and time-domain scattering by nonuniform truncated arrays. IEEE Antennas Propagat. 36: 29-43; 1994.

[16] Cohen, L. Time-frequency distributions--a review. Proc. IEEE, 77: 941-981; 1989.

[17] Lim, J.S.; Oppenheim, A.V. Advanced topics in signal processing. New Jersey: Prentice Hall; 1988.

[18] Press, W.H.; Flannery, B.P.; Teukolsky, S.A.; Vetterling, W.T. Numerical Recipes in C--The art of scientific computing. New York: Cambridge University Press; 1988.

[19] Schroeder, M.R. New method of measuring reverberation time. J. Acoust. Soc. Am. 37: 409-412, 1965.

[20] Davy, J.L. The variance of impulse decays. Acustica 44: 51-56, 1980.

[21] Johnk, R.T.; Ondrejka, A.R. Time-domain measurements of the reverberation characteristics and shielding effectiveness of a small aircraft. URSI National Radio Science Meeting: 127, 1994.

[22] Knudsen, V.O.; Delsasso, L.P.; Leonard, R.W. Reverberation-room acoustics-effects of various boundary conditions. J. Acoust. Soc. Am. 42: 953-965, 1967.

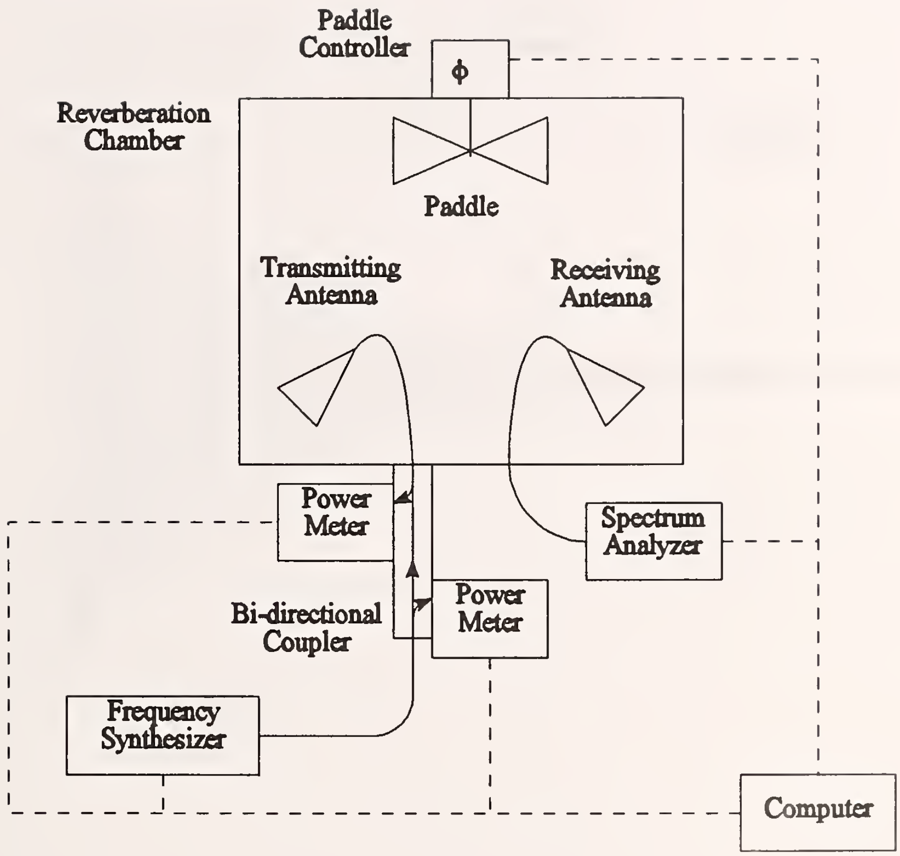

Figure 1. Traditional measurement configuration.

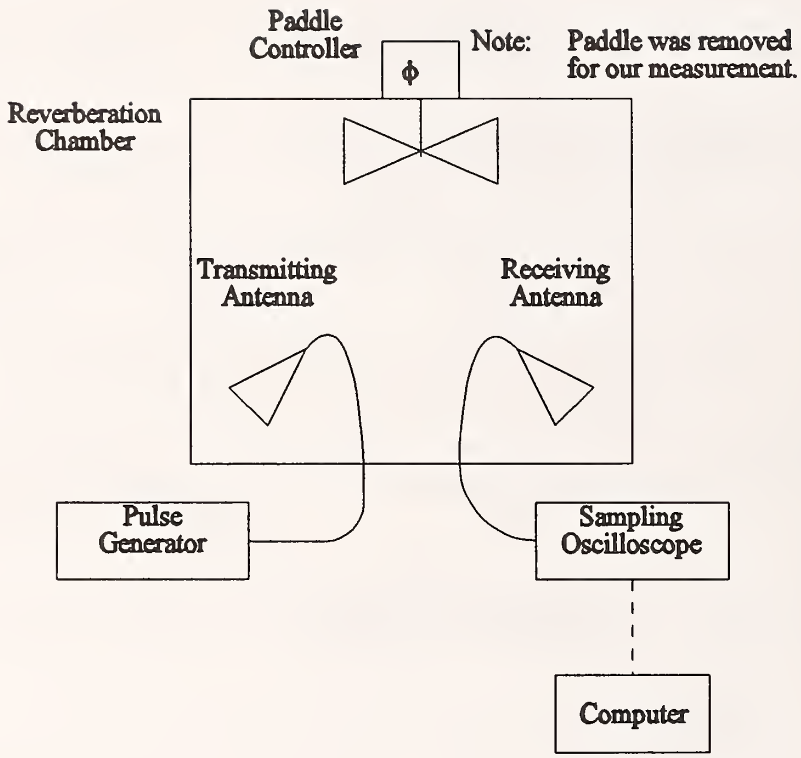

Figure 2. Proposed NIST time-domain measurement configuration.

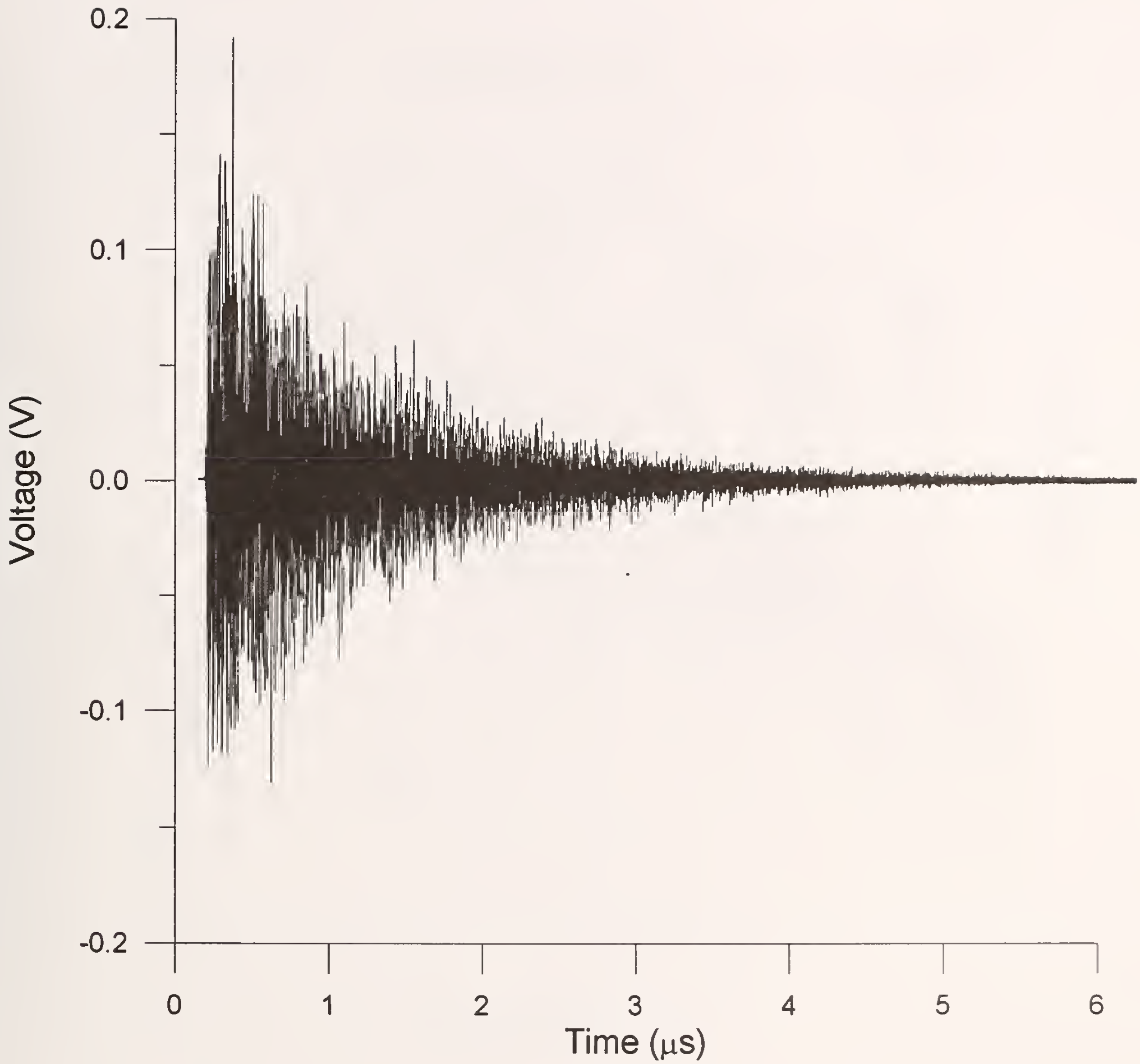

Figure 3. Sampled impulse response of NIST chamber.

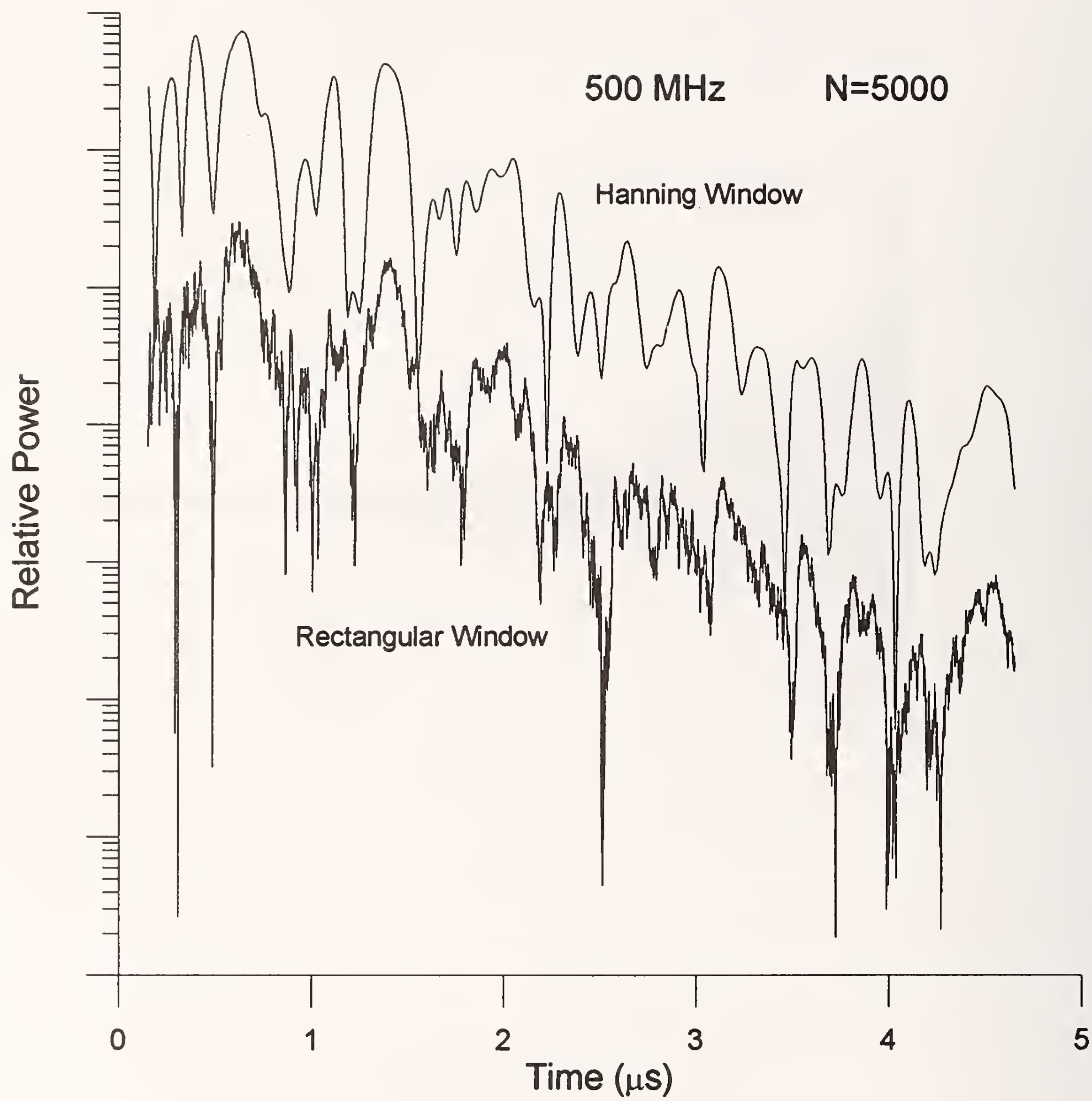

Figure 4. Effect of tapered window on processed results.

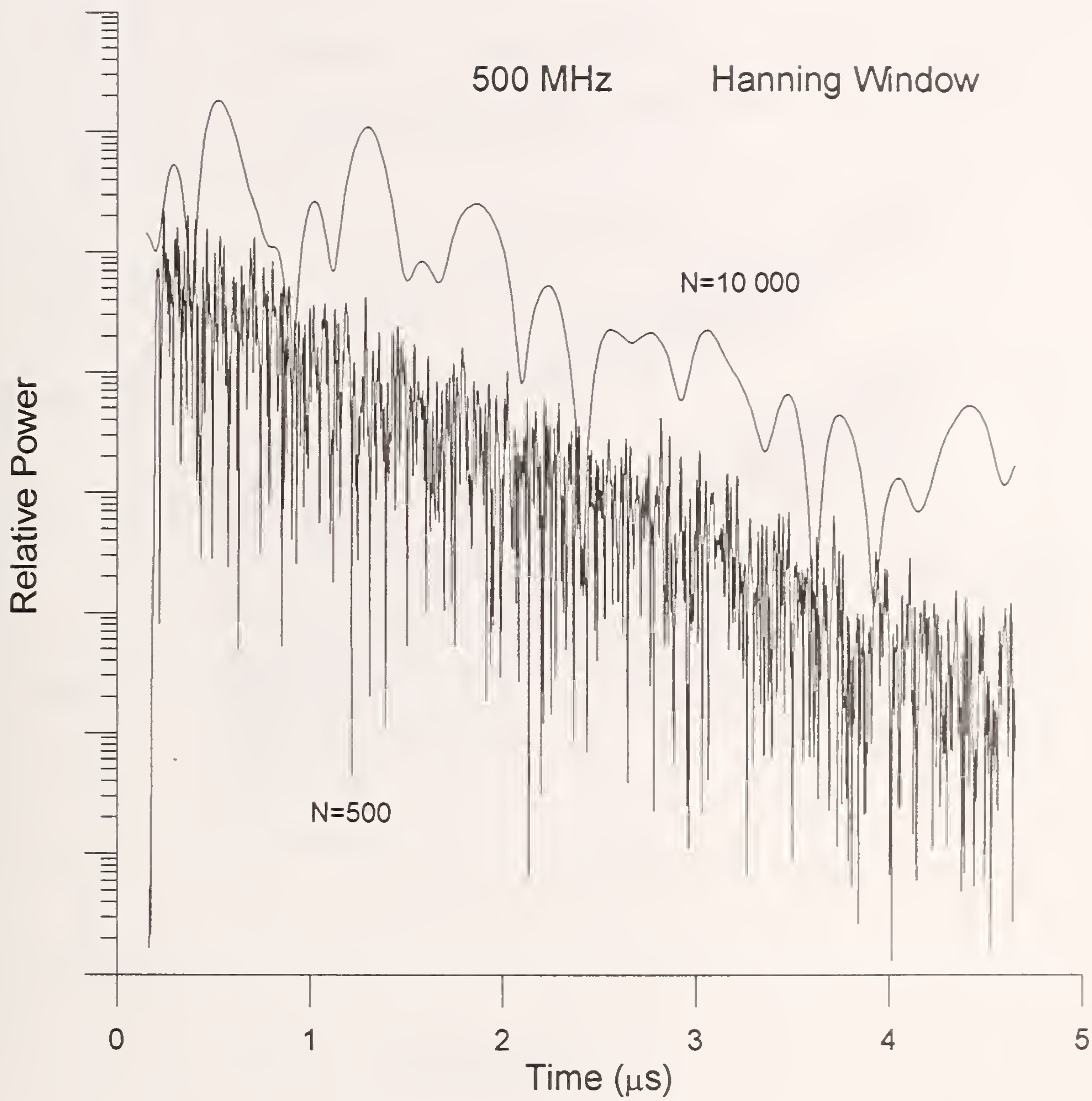

Figure 5. Effect of window size on processed results.

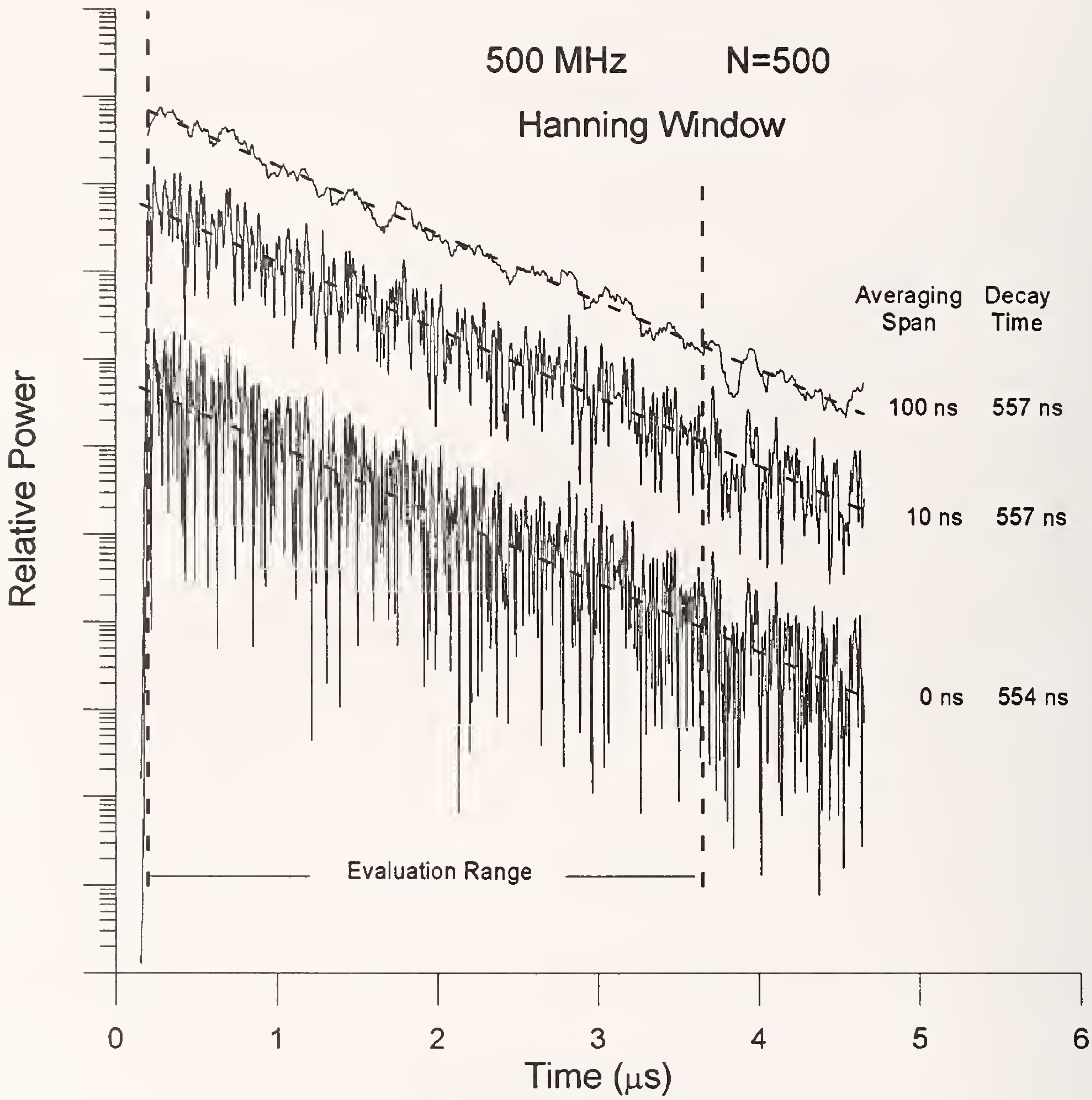

Figure 6. Time averaged results.

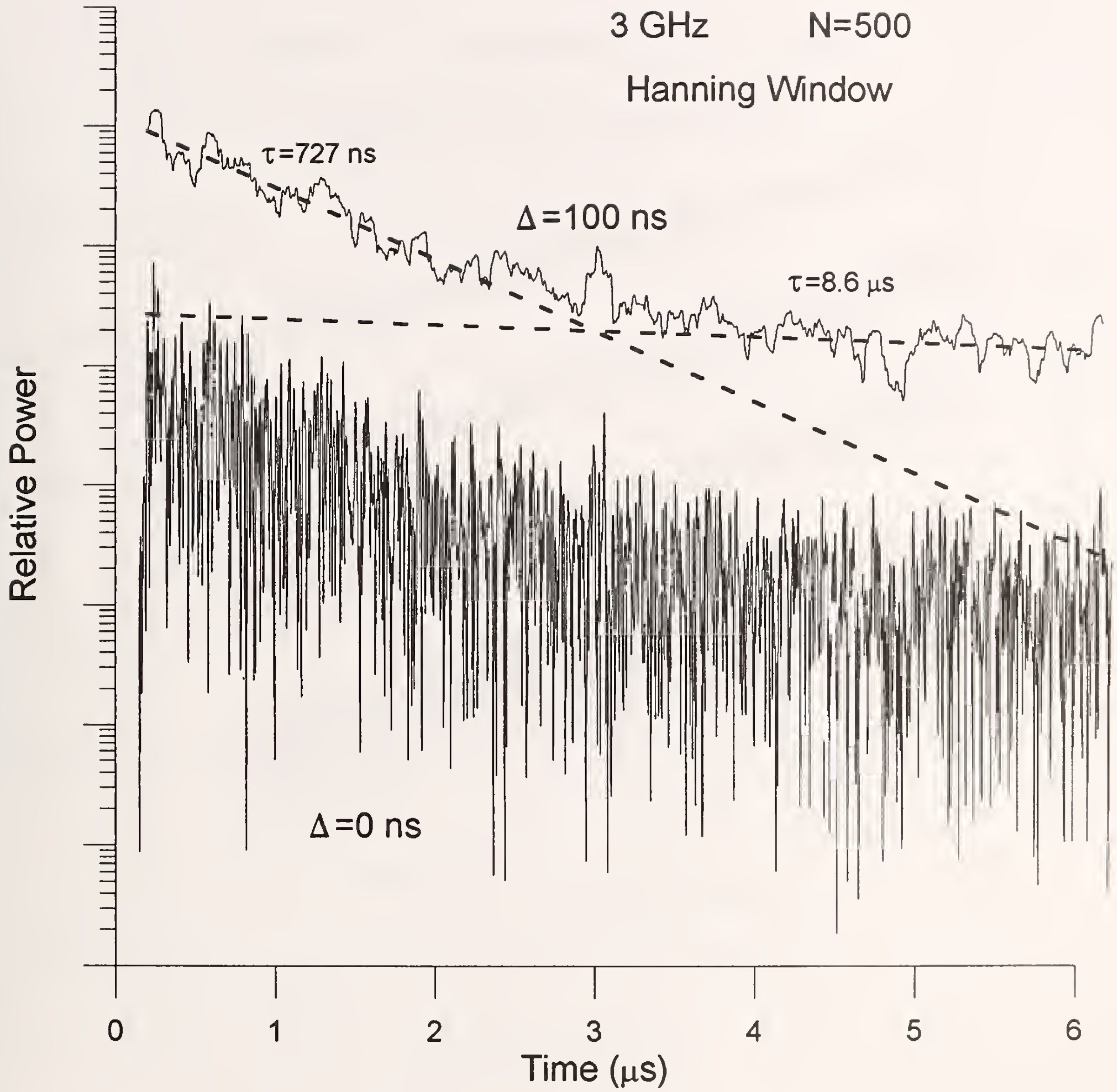

Figure 7. Noise floor of the measurement system.

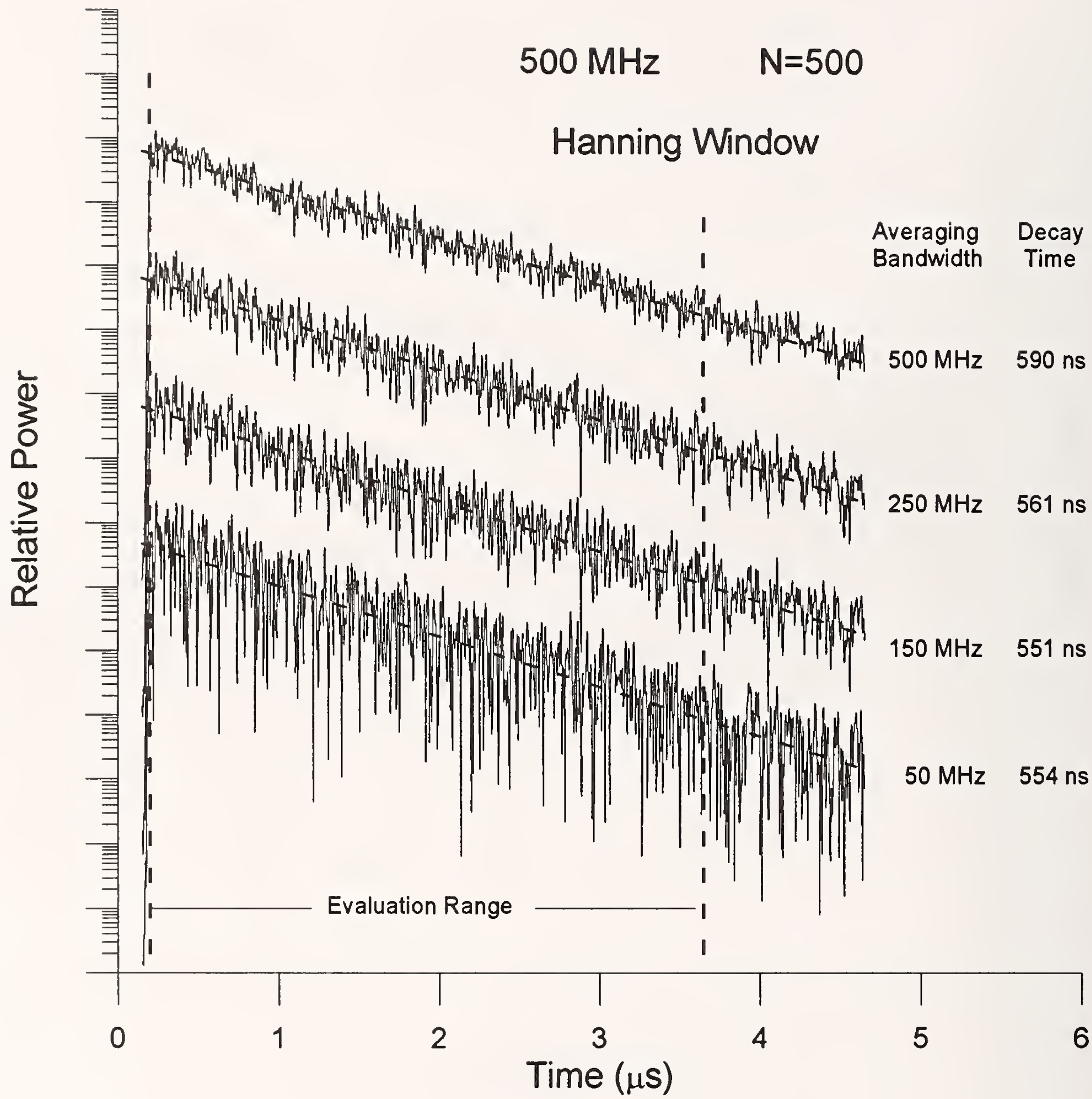

Figure 8. Results of frequency averaging with a short time window.

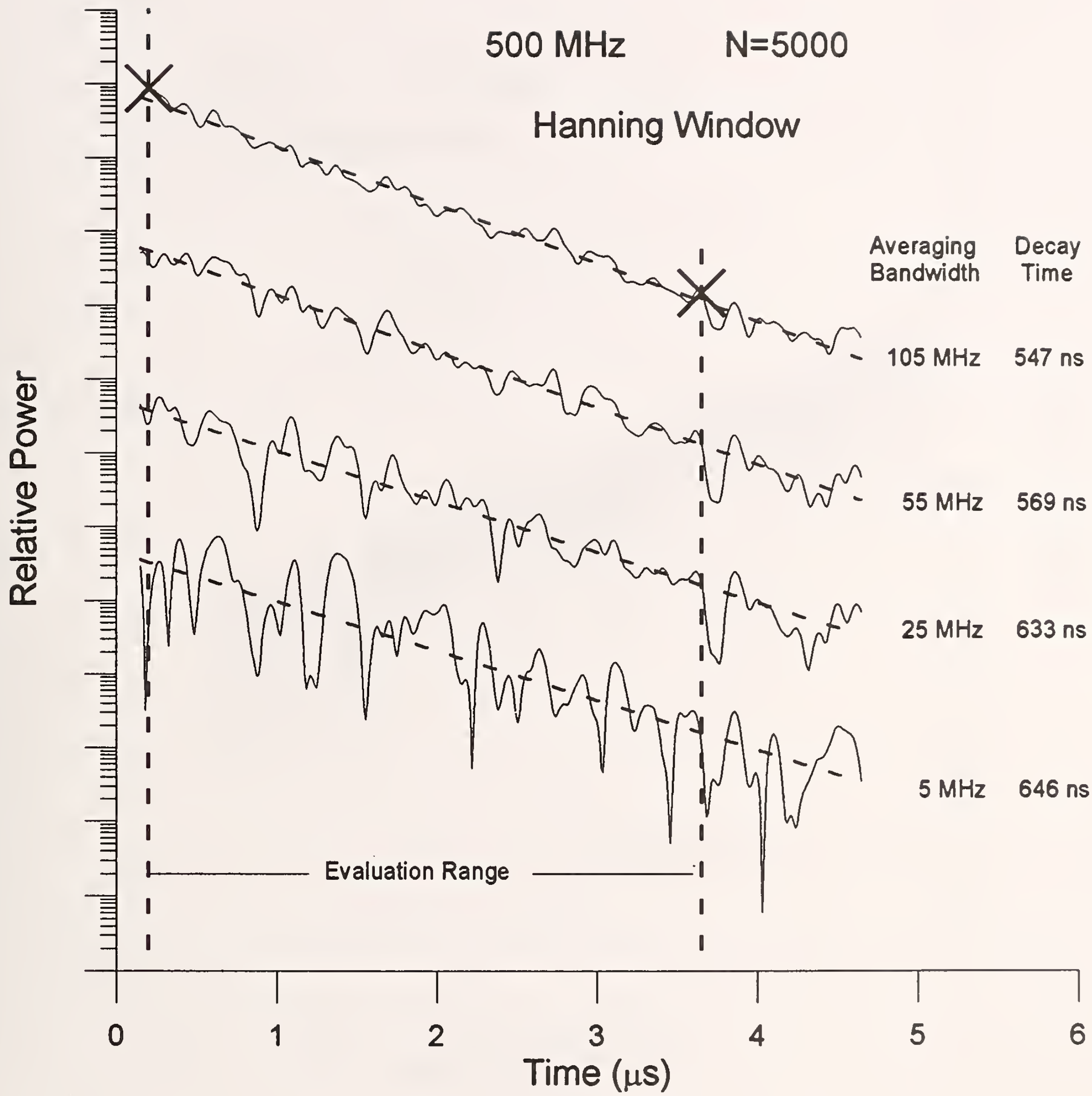

Figure 9. Results of frequency averaging with a long time window.

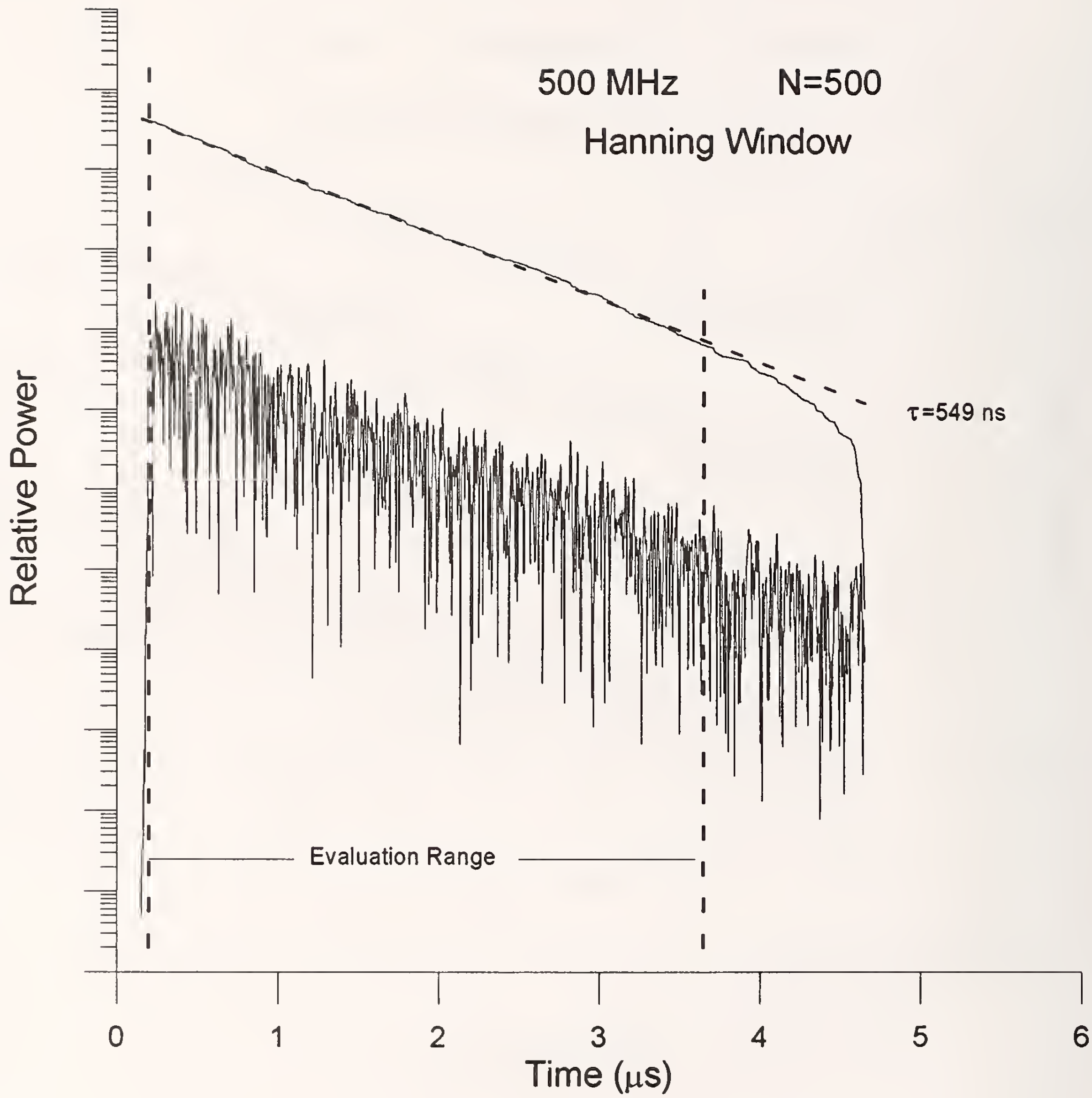

Figure 10. The Integrated Impulse Response Method (short time window).

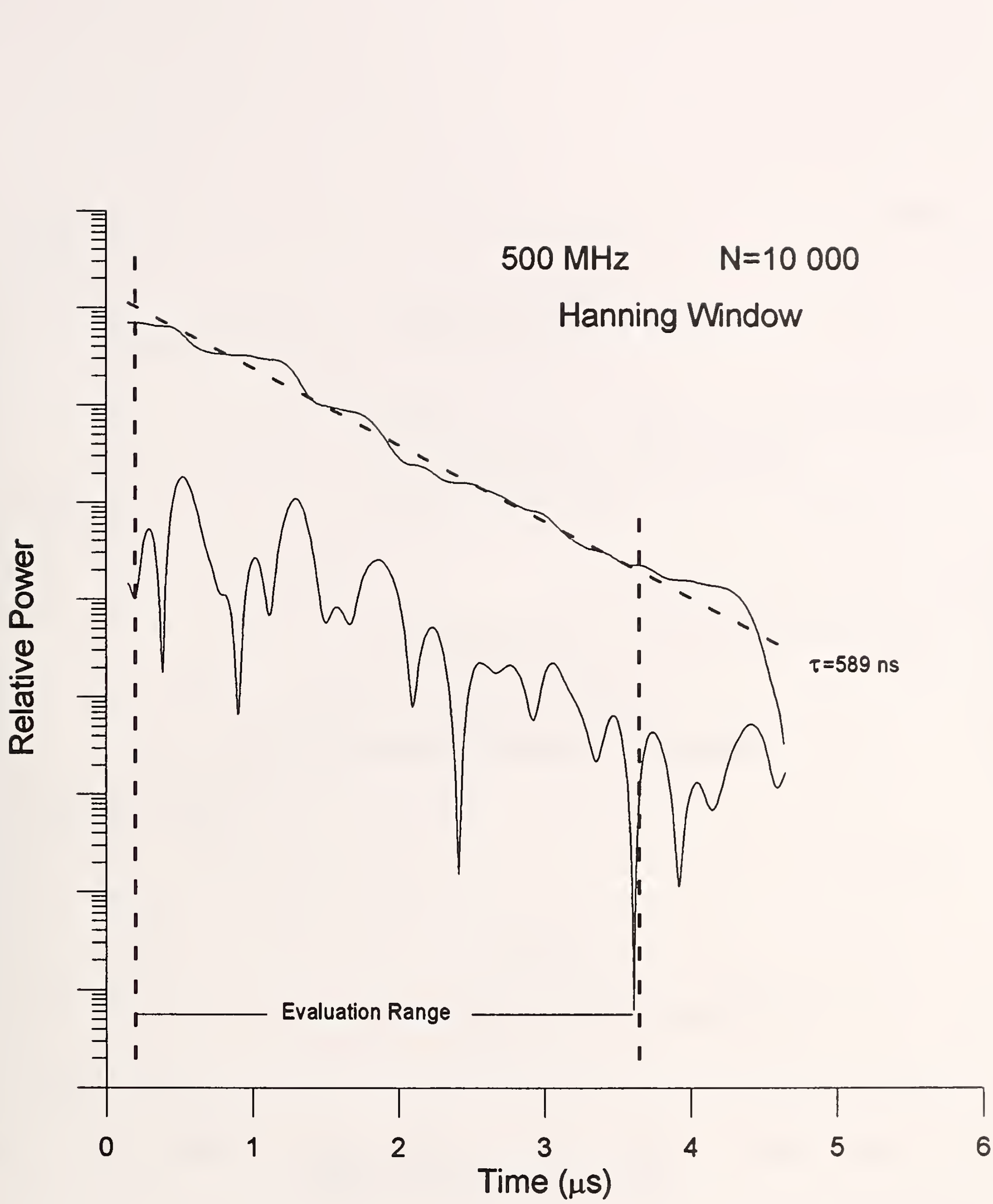

Figure 11. The Integrated Impulse Response Method (long time window).

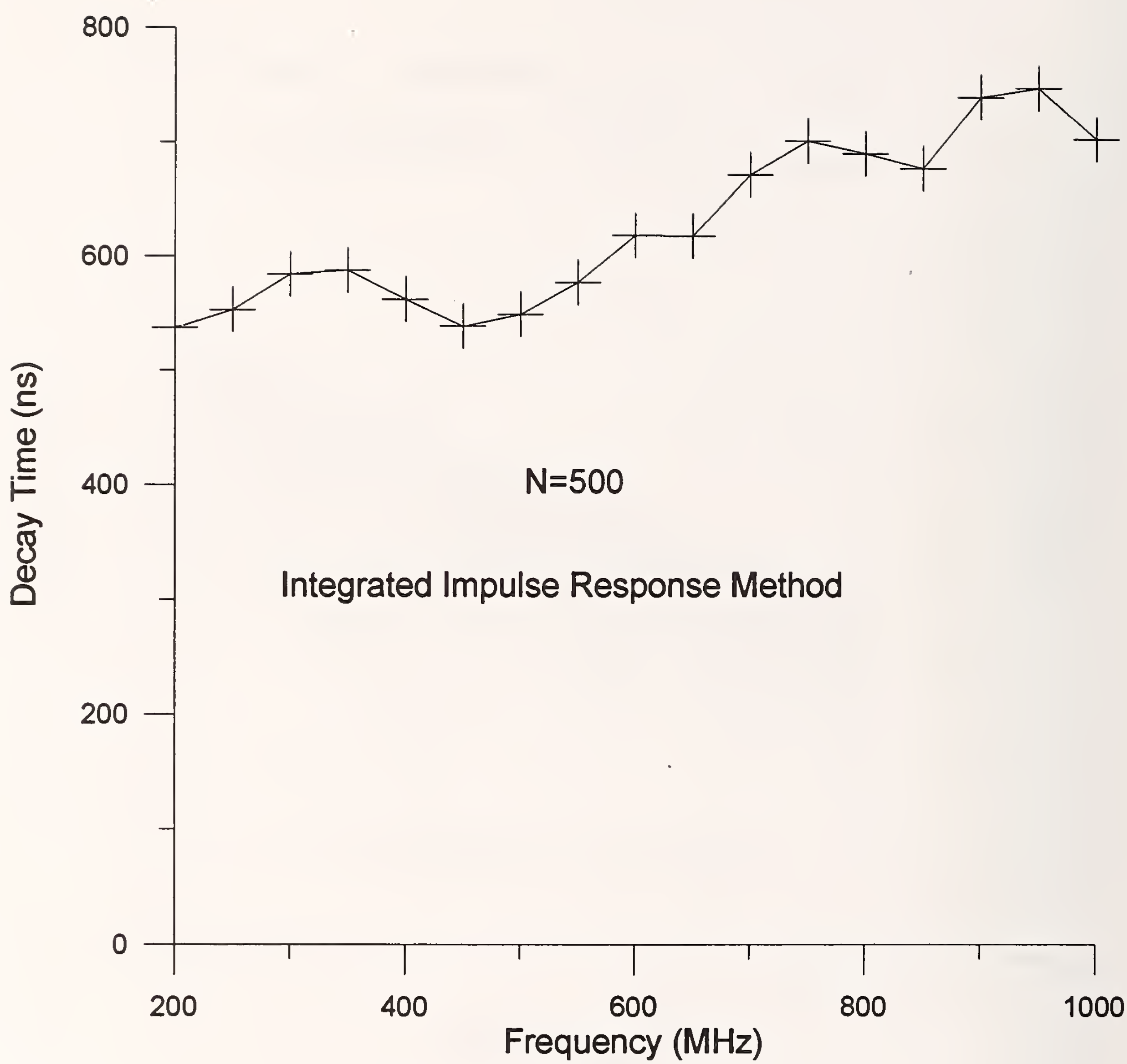

Figure 12. Calculated decay times versus frequency.

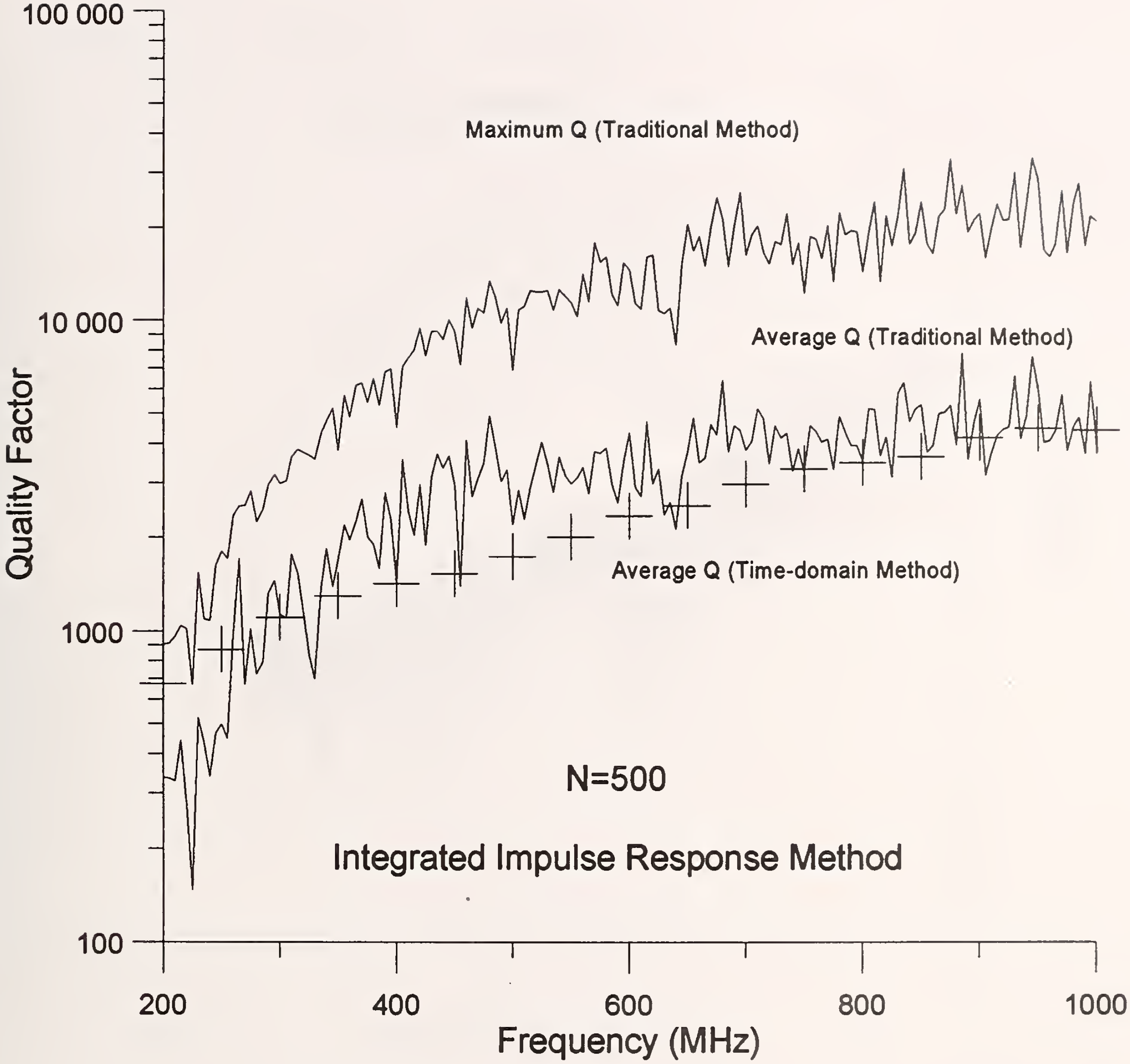

Figure 13. Comparison of Q estimates using traditional and time-domain methods.

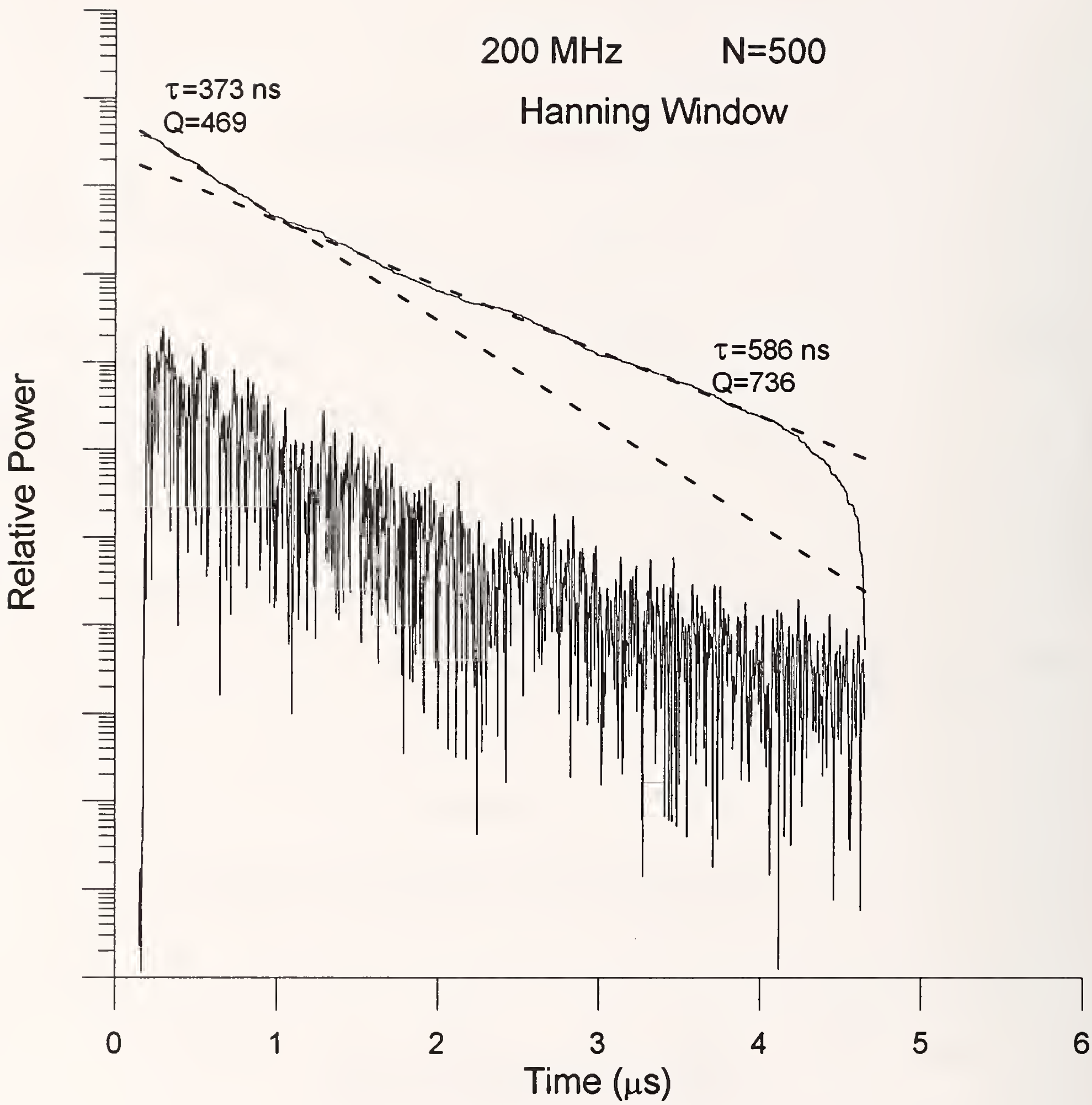

Figure 14. Strange behavior at 200 MHz. (Multiple decay rates?)

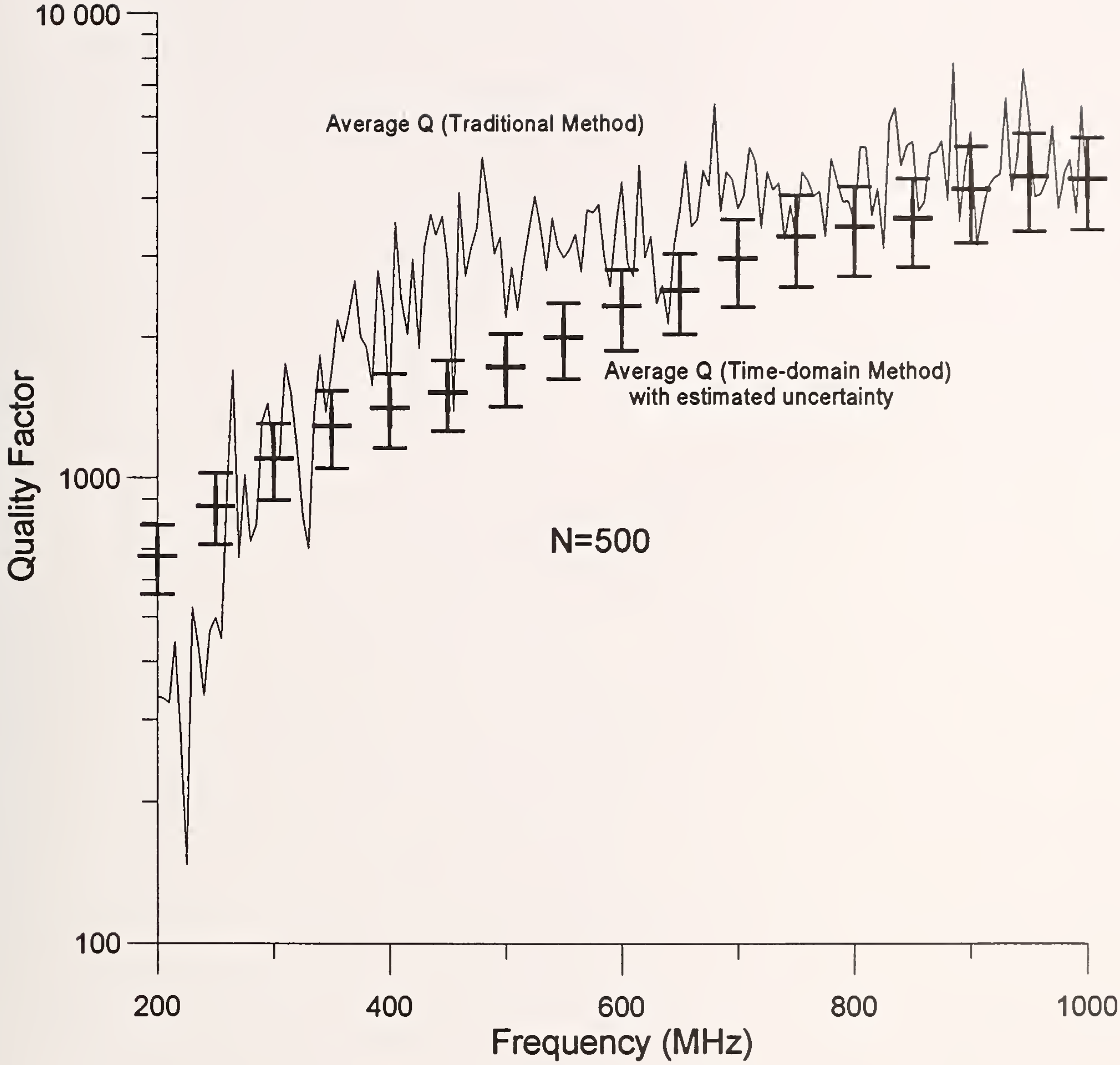

Figure 15. Estimated accuracy of time-domain Q measurement method.

• U.S. GOVERNMENT PRINTING OFFICE 1998-0-774-018-40016

NIST *Technical Publications*

Periodical

Journal of Research of the National Institute of Standards and Technology—Reports NIST research and development in those disciplines of the physical and engineering sciences in which the Institute is active. These include physics, chemistry, engineering, mathematics, and computer sciences. Papers cover a broad range of subjects, with major emphasis on measurement methodology and the basic technology underlying standardization. Also included from time to time are survey articles on topics closely related to the Institute's technical and scientific programs. Issued six times a year.

Nonperiodicals

Monographs—Major contributions to the technical literature on various subjects related to the Institute's scientific and technical activities.

Handbooks—Recommended codes of engineering and industrial practice (including safety codes) developed in cooperation with interested industries, professional organizations, and regulatory bodies.

Special Publications—Include proceedings of conferences sponsored by NIST, NIST annual reports, and other special publications appropriate to this grouping such as wall charts, pocket cards, and bibliographies.

Applied Mathematics Series—Mathematical tables, manuals, and studies of special interest to physicists, engineers, chemists, biologists, mathematicians, computer programmers, and others engaged in scientific and technical work.

National Standard Reference Data Series—Provides quantitative data on the physical and chemical properties of materials, compiled from the world's literature and critically evaluated. Developed under a worldwide program coordinated by NIST under the authority of the National Standard Data Act (Public Law 90-396). NOTE: The Journal of Physical and Chemical Reference Data (JPCRD) is published bi-monthly for NIST by the American Chemical Society (ACS) and the American Institute of Physics (AIP). Subscriptions, reprints, and supplements are available from ACS, 1155 Sixteenth St., NW, Washington, DC 20056.

Building Science Series—Disseminates technical information developed at the Institute on building materials, components, systems, and whole structures. The series presents research results, test methods, and performance criteria related to the structural and environmental functions and the durability and safety characteristics of building elements and systems.

Technical Notes—Studies or reports which are complete in themselves but restrictive in their treatment of a subject. Analogous to monographs but not so comprehensive in scope or definitive in treatment of the subject area. Often serve as a vehicle for final reports of work performed at NIST under the sponsorship of other government agencies.

Voluntary Product Standards—Developed under procedures published by the Department of Commerce in Part 10, Title 15, of the Code of Federal Regulations. The standards establish nationally recognized requirements for products, and provide all concerned interests with a basis for common understanding of the characteristics of the products. NIST administers this program in support of the efforts of private-sector standardizing organizations.

Consumer Information Series—Practical information, based on NIST research and experience, covering areas of interest to the consumer. Easily understandable language and illustrations provide useful background knowledge for shopping in today's technological marketplace.

Order the **above** *NIST publications from: Superintendent of Documents, Government Printing Office, Washington, DC 20402.*

Order the **following** *NIST publications—FIPS and NISTIRs—from the National Technical Information Service, Springfield, VA 22161.*

Federal Information Processing Standards Publications (FIPS PUB)—Publications in this series collectively constitute the Federal Information Processing Standards Register. The Register serves as the official source of information in the Federal Government regarding standards issued by NIST pursuant to the Federal Property and Administrative Services Act of 1949 as amended, Public Law 89-306 (79 Stat. 1127), and as implemented by Executive Order 11717 (38 FR 12315, dated May 11, 1973) and Part 6 of Title 15 CFR (Code of Federal Regulations).

NIST Interagency Reports (NISTIR)—A special series of interim or final reports on work performed by NIST for outside sponsors (both government and non-government). In general, initial distribution is handled by the sponsor; public distribution is by the National Technical Information Service, Springfield, VA 22161, in paper copy or microfiche form.

U.S. Department of Commerce
National Institute of Standards and Technology
325 Broadway
Boulder, Colorado 80303-3328